WOOD RESEARCH doi.org/10.37763/wr.1336-4561/68.2.334347
ISSN 1336-4561 e-ISSN 2729-8906
68(2): 2023 334-347 pp.

DETERMINATION OF MODE I FRACTURE PROPERTIES OF EUROPEAN SPRUCE

MARIJA TODOROVIĆ[1], MATHIEU KOETSIER[2], NAĐA SIMOVIĆ[1], IVAN GLIŠOVIĆ[1], MARKO PAVLOVIĆ[2]

[1]UNIVERSITY OF BELGRADE, SERBIA
[2] DELFT UNIVERSITY OF TECHNOLOGY, THE NETHERLANDS

(RECEIVED OCTOBER 2022)

ABSTRACT

In this paper an efficient procedure for obtaining a cohesive law for Mode I timber fracture (crack opening), based on the Double Cantilever Beam (DCB) tests is given. DCB tests were performed on ten European spruce specimens in order to determine the energy release rate vs crack length (R curves). Two crucial parameters - crack length during the experiment and the crack tip opening displacement were obtained using 2D Digital Image Correlation (DIC) technique. In order to determine accurate fracture resistance (R curve), procedure which includes calculating cumulative released energy was employed. The cohesive law for Mode I fracture of wood was obtained by differentiation of the strain energy release rate as a function of the crack tip opening displacement. This cohesive law is further implemented in the successful numerical modelling of failure modes in large-scale end-notched glulam beams which were experimentally tested in four-point bending configuration.

KEYWORDS: Mode I fracture, wood, DCB, DIC, R curve.

INTRODUCTION

As many other materials, wood develops damage process zones in the case of propagating cracks, causing toughness to change as the crack propagates. Fibre-bridging effect is responsible for the process zone development in wood. Crack propagation experiments in materials which develop fibre bridging across the crack start with a machined notch that has no process zone (Nairn and Matsumoto 2009). As the load is applied fibre-bridging zone develops with two crack tips. One crack tip is the actual crack tip and one is at the edge of the fibre-bridging zone defined as the notch root (Fig. 1a). The distance between them represents the process zone length. At the initial point of fracture, the crack tip moves while

the notch root remains stationary and toughness is low. As the process zone develops, toughness tends to raise with crack growth, since unbroken wood fibres that connect crack surfaces can carry load. Once the fibres break, the process zone length stabilizes (steady-state crack propagation), propagating together with the developing crack, and the toughness becomes constant. The fracture resistance curve (R curve) is a representation of the toughness of the material in relation to crack propagation. In order to correctly describe the fracture process of any material, including wood, an accurate definition of the R curve is necessary.

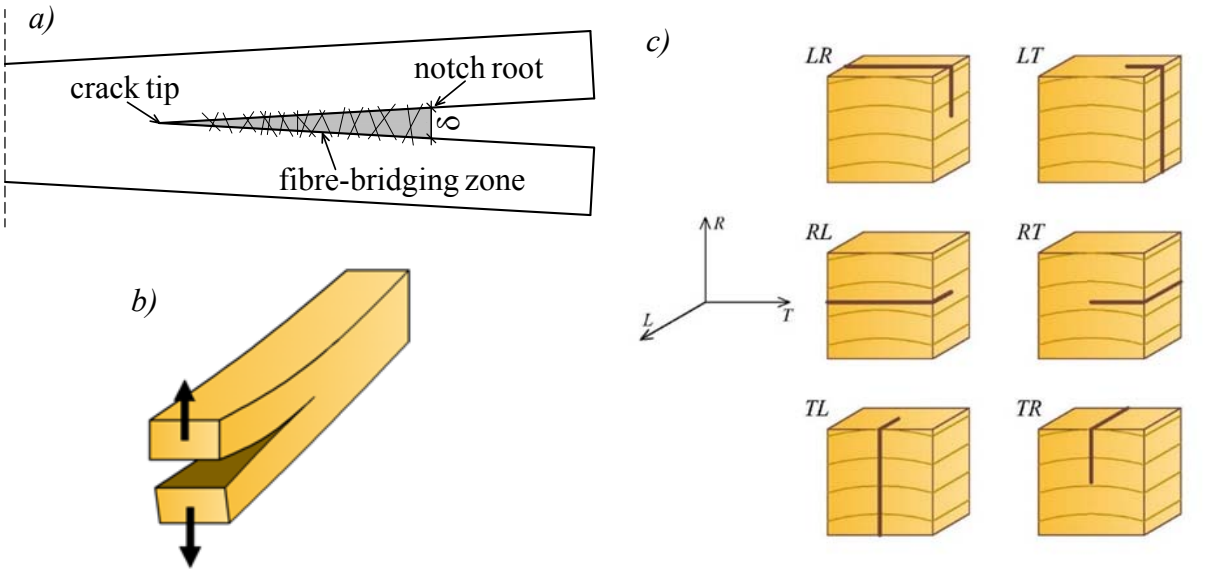

Fig. 1: a) Crack tip region with fibre-bridging zone, b) Mode I fracture, c) Fracture planes in wood.

Comprehensive research has been undertaken on end-notched timber beams in order to satisfy construction requirements of reduced height of timber beams at the supports (Todorović et al. 2019, 2022). Dominant failure mechanism of end-notched beams is proved to be Mode I fracture caused by excessive tensile stress perpendicular to the grain of timber (Fig. 1b), as confirmed by Jockwer (2014). In order to accurately describe the behaviour of end-notched timber beams, it is necessary to determine fracture parameters, that is, cohesive law for Mode I fracture of wood. Different methods have been used so far by the researchers for determination of Mode I fracture of wood, such as: three-point bending test (Morel et al. 2005, Dourado et al. 2015), single-edge-notch specimen (Nakao et al. 2012), wedge-splitting test (Dubois et al. 2012, Ostapska and Malo 2020, 2021), tapered double cantilever beam test (Vasic and Smith 2002, de Moura and Dourado 2018), and double cantilever beam test (Yoshihara and Kawamura 2006, de Moura et al. 2008, Zhao et al. 2017).

In this paper, an experimental procedure for measuring R curves of wood is explained. Double Cantilever Beam (DCB) tests were performed in order to determine Mode I fracture (crack opening) properties of spruce wood. In accordance with the large-scale experiments performed on the end-notched beams crack propagation is considered in the radial-longitudinal direction - RL direction (Fig. 1c). In order to overcome the main obstacle occurring with the DCB tests, which is crack length measurement, Digital Image Correlation (DIC) method was

applied for recording the crack opening and propagation. Jamaaoui et al. (2017) demonstrated that DIC method can be successfully used to estimate the crack length and the mechanical state at the crack tip.

Procedure for energy release rate explained by Wilson et al. (2013) was used in this research to obtain R curves (energy release rate vs crack length). This approach can be applied to fracture mechanics tests with wood as a linear orthotropic viscoelastic material. In elastic materials, the fracture energy is released only due to the development of the damage process zone and the crack growth in the crack plane, but no energy is released due to the non-linear (plastic or damage) behaviour of the materials surrounding the crack plane. This procedure includes calculating the cumulative energy released up to the certain value of the loading point displacement. In order to determine cumulative energy, unloading from this point would be required. As authors Wilson et al. (2013) argue in their paper, the fibre-bridging zone would interfere with the unloading and the curve would not return to the origin. Furthermore, authors explain that energy from such crack plane interference during unloading is not a part of the energy released during monotonic crack propagation, and it should not be a part of the cumulative released energy. Therefore, the proposed method assumes that the unloading would return to the origin displacement. The obtained cumulative energy can be cross-plot in the function of the corresponding crack length. The R curves represent the slope of cumulative energy - crack length curve. The cohesive energy G_f was determined from the R curves. Based on these results, cohesive law for Mode I fracture was defined.

Value of the experimentally obtained cohesive fracture energy and cohesive law was further employed for the accurate numerical modelling of end-notched glulam beams which were previously experimentally tested in bending to the point of failure, as a part of a larger experimental investigation.

MATERIALS AND METHODS

Double cantilever beam (DCB) test

Altogether 10 specimens made from European spruce (*Picea abies*) were tested as DCB to the point of failure at the TU Delft, Faculty of Civil Engineering and Geosciences, Department of Engineering Structures. The specimens were denoted as S1-S10 and had nominal dimensions of 20 x 30 x 300 mm. They were made from spruce timber classified in the strength class C22 according to EN 338 (2009). The specimens were made out of the same wood as were the large-scale end-notched beams, so that the results could be used in further numerical analysis of Mode I fracture. Material tests of timber were previously performed at Faculty of Civil Engineering, University of Belgrade are listed in Tab. 1. Density was determined in accordance with ISO 13061-2 (2014), while bending strength, modulus of elasticity, shear strength and tensile strength perpendicular to the grain were determined in accordance with EN 408 (2012) on small clear wood samples. In order to account for the size effect, the tested bending strength value was adjusted according to EN 384 (2010).

Tab. 1: Material properties of spruce timber.

Density ρ (kg·m^{-3})	Modulus of elasticity E_m (N·mm^{-2})	Bending strength f_m (N·mm^{-2})	Shear strength f_v (N·mm^{-2})	Tensile strength perpendicular to the grain $f_{t,90}$ (N·mm^{-2})
411.1	10749.5	39.1	5.85	1.15

DCB specimen geometry and testing set up are presented in Fig. 2a. The initial 100 mm long crack was formed using a saw with 1 mm thickness. Steel pins with a diameter of 3 mm were used for joining the specimens to the loading fixture. Universal testing machine UTM-25 was employed for the experimental testing (Fig. 2b). Load was applied monotonically with a displacement-controlled rate of 5 mm·min^{-1}. Load and displacement were recorded using the loading cell with a frequency of 2 Hz. All tests were performed under ambient conditions (at a temperature of about T = 20ºC and a relative humidity of about RH = 65%). Using a digital hygrometer moisture content was measured in all the specimens and it had values in a range of 11.0% to 11.9%.

2D DIC method was employed for crack length measurement, as well as the measurement of crack opening during the testing. The main problem of this experiment is accurate crack length reading which is of outmost importance for the definition of R curves. To overcome this problem, images recorded with a 51Mpx camera were analysed with GOM correlate software. By defining two curves on the upper and lower crack surfaces which are easily visible during the analysis, and measuring the separation between these curves allowed for the accurate crack length reading at each loading step.

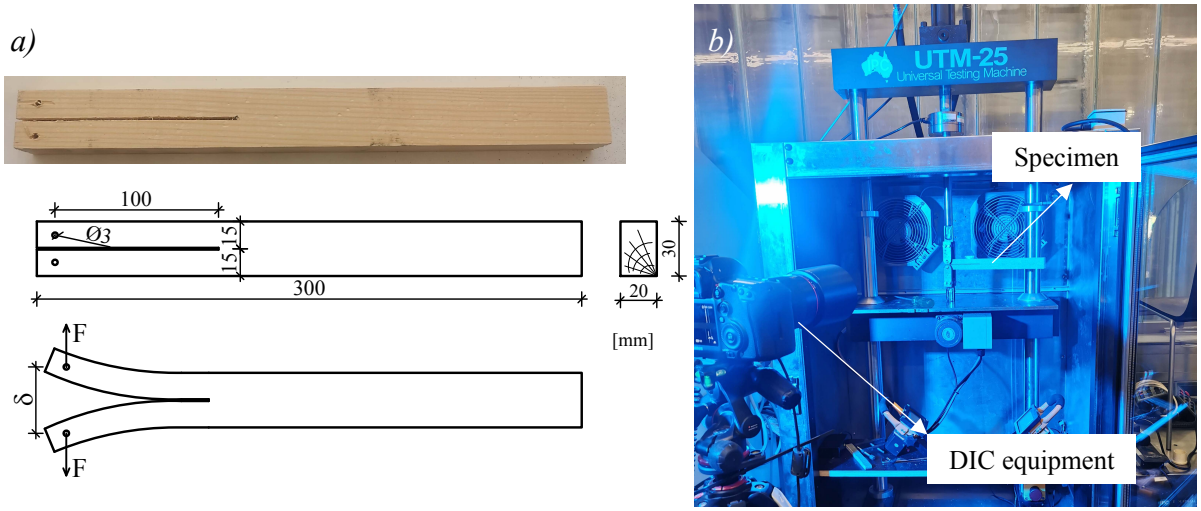

Fig. 2: a) DCB specimen geometry and testing method, b) Experimental set-up.

Energy release rate was calculated as suggested by Wilson et al. (2013). The cumulative energy released up to the certain value of the loading point displacement δ (presented as shaded area in Fig. 3) was determined as follows:

$$U(\delta) = \int_{\delta_0}^{\delta} F(x)dx - \frac{1}{2}F(\delta)(\delta - \delta_0) \quad (1)$$

where: U - cumulative energy, δ - loading point displacement, δ_0 - origin displacement, F - force and $F(\delta)$ - force corresponding to δ.

Afterwards, cumulative energy is cross-plot in the function of the corresponding crack length (Fig. 3). Crack lengths were read from the DIC images for the corresponding force and displacement during the experiment. Finally, the R curves are determined as the slope of cumulative energy - crack length curve:

$$R = \frac{1}{b}\frac{dU(a)}{da} \tag{2}$$

where: R - energy release rate, b - specimen width and a - crack length.

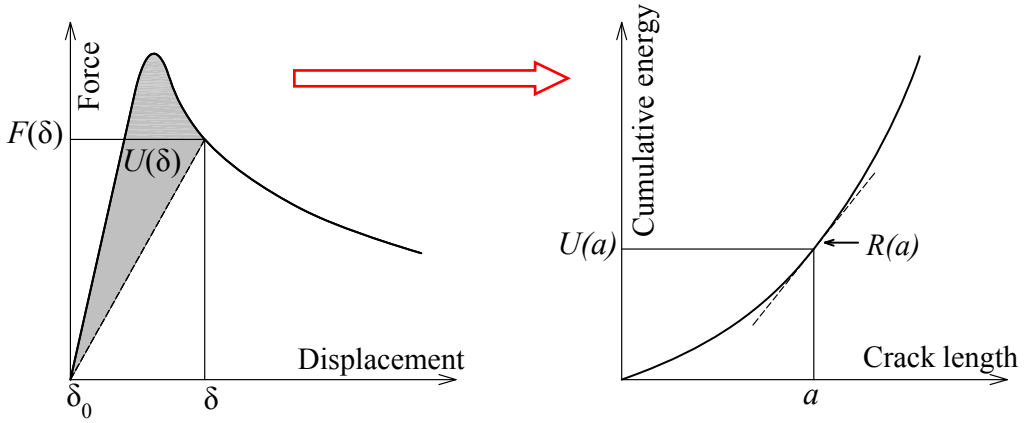

Fig. 3: Procedure for determining R curves based on cumulative released energy (Wilson et al. 2013).

Numerical modelling of end-notched timber beams

The experimental research on five end-notched glulam beams was conducted at the Laboratory of Structures, Faculty of Civil Engineering, University of Belgrade. The glulam beams were made from spruce timber classified in the strength class C22 according to EN 338 (2009). The beams were denoted as U6-U10 with dimensions of 100 x 220 x 4000 mm. At the notched ends, the height of the beams was reduced to 110 mm (by half) and the length of notches was 250 mm (Fig. 4). The beams were tested to failure under monotonic load in four-point bending configuration, in accordance with EN 408 (2012), over a simply supported span of 3750 mm. Roller bearings were used at the supports and at the load application points. The effects of local indentation at the load application and support positions were minimized by placing steel plates.

Before the tests were performed, the beams were conditioned at a temperature of T = 20 ± 2ºC and a relative humidity of RH = 65 ± 5% for seven days. The load was applied monotonically at a stroke-controlled rate so as to cause failure of the beams in approximately 5 min. The load was applied using a hydraulic jack and recorded with a compression load cell. The load was transformed from one point to two points with a steel beam. Linear variable differential transducers (LVDTs) were used for the measurement of mid-span deflections. The deformation data from LVDTs and corresponding load data from the load cell were recorded by a computerized data acquisition system. Self-weight of hydraulic jack and steel

beam was added to the recorded load as 1.3 kN. Geometry and loading of the beams are presented in Fig. 4.

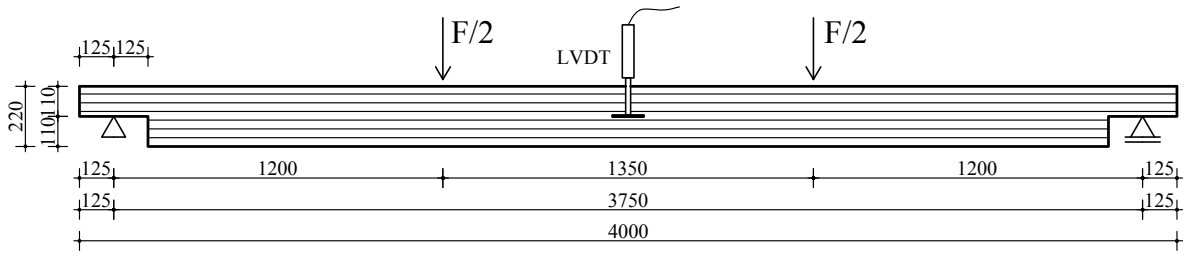

Fig. 4: Geometry and loading of end-notched beams.

Numerical simulation of tested end-notched beams was created in the finite element software Abaqus ver. 6.13. Special attention was put into the modelling of crack opening and its growth which was simulated using a nonlinear fracture mechanics approach via Cohesive Zone Modelling (CZM) option available in this software. Equivalent approach to FE modelling of notched beams was applied by Oudjene et al. (2016).

Geometry of the beams, loading and boundary conditions were modelled so as to correspond to the experimental set-up (Fig. 4). Only half of the beam was modelled with appropriate symmetry constraints applied. Laminations were considered as separate parts, with perfect connection assumed at bonding interfaces, since no bond-line failures were recorded during the experimental testing. The end-notched beams were modelled as C3D8R finite elements (eight-node solid finite elements with reduced integration), with each lamination having two finite elements throughout its thickness (finite element size 16 mm). Steel plates at the supports and loading points were modelled using S4R finite elements (four-node shell finite elements with reduced integration) with a size of 5 mm. Execution of the model involved a static small displacement analysis consisting of a series of vertical displacement-controlled increments applied at the loading plates. Boundary conditions, symmetry conditions, position of the loading point, position of the embedded CZM interaction and mesh of the FE model are shown in Fig. 5.

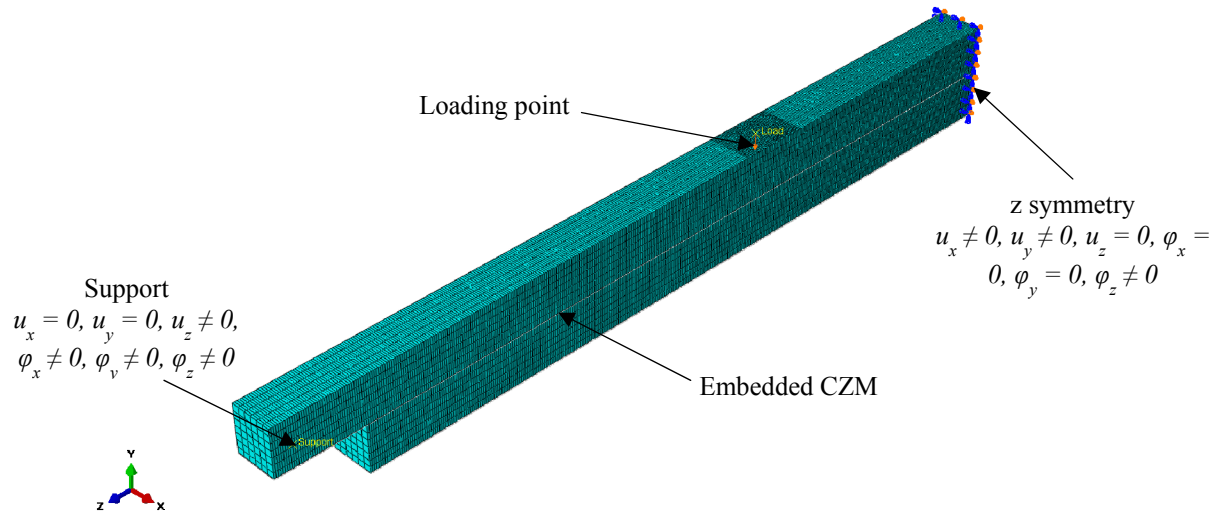

Fig. 5: FE model of end-notched glulam beam.

Timber was modelled as an orthotropic linear-elastic material. The material parameters (E - moduli of elasticity, G - shear moduli, ν - Poisson's ratio) that describe the wood behaviour were taken from previously performed experimental tests and based on relations given by Bodig and Jayne (1982), shown in Tab. 2.

Tab. 2: Wood material parameters.

Parameter	E_L ($N \cdot mm^{-2}$)	E_R ($N \cdot mm^{-2}$)	E_T ($N \cdot mm^{-2}$)	G_{LR} ($N \cdot mm^{-2}$)	G_{LT} ($N \cdot mm^{-2}$)	G_{RT} ($N \cdot mm^{-2}$)	ν_{LR} (-)	ν_{LT} (-)	ν_{RT} (-)
Value	10 750	860	538	768	724	77	0.37	0.42	0.47

A damage initiation criterion of maximum nominal stress and a fracture energy-based damage evaluation criterion with exponential softening were used to simulate the cohesive crack growth in the expected crack plane. Input values were adopted based on the results of the performed DCB tests.

RESULTS AND DISCUSSION

DCB test results

All DCB specimens experienced expected Mode I fracture - crack opening, caused by excessive tensile stress perpendicular to the grain of wood. Typical failure of tested specimens is presented in Fig. 6.

Fig. 6: Typical Mode I failure (crack opening) mechanism of tested specimens S1-S10.

Force-displacement curves of all tested specimens are presented in Fig. 7. Behaviour of the specimens was entirely linear until ultimate load corresponding to the initial crack opening was reached, as it can be seen from the curves, which show a sudden drop in load. Afterwards, crack propagation and growth lead to a complete separation of the beams in two parts, with generally clear and straight surfaces between two separated parts.

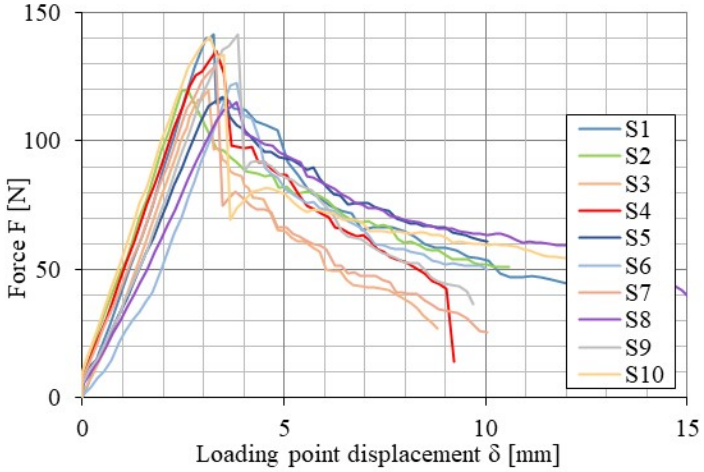

Fig. 7: Force-displacement curves.

After implementing the proposed procedure for energy release rate, cumulative energy vs crack length and R curves of tested specimens were calculated and presented in Fig. 8 and Fig. 9. The recorded data of force-displacement was comprehensive enough to be easily integrated. For each step of loading, corresponding crack length was read from the DIC images. Differentiation of the $U(a)$ curve was performed by fitting with adequate third-degree polynomial curve with average $R^2 = 0.996$, which was afterwards easily numerically differentiated.

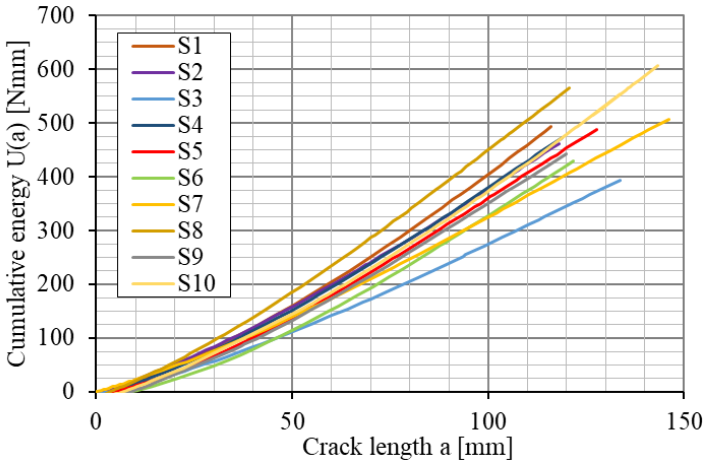

Fig. 8: Cumulative energy-crack length curves.

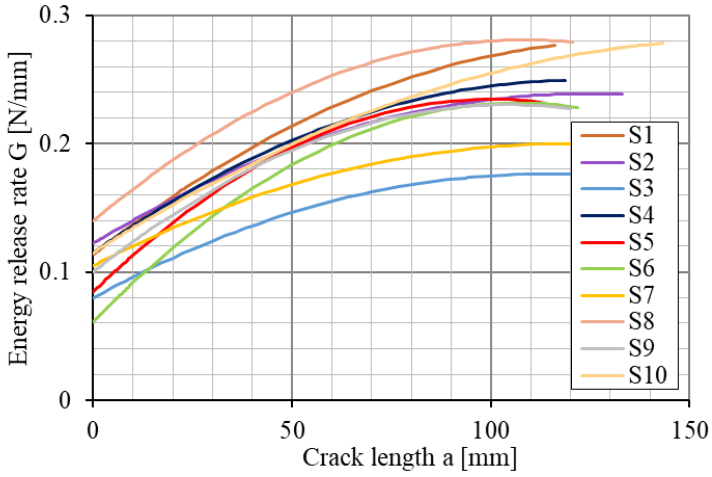

Fig. 9: R-curves.

The cohesive energy or critical value of energy release rate at propagation - G_f corresponds to the plateau value of the R curve (Coureau et al. 2013). This parameter values are estimated once the toughness stabilized after fibre-bridging process completed and R curves appear to be reaching the steady state. The experimental results for cohesive energy of tested spruce specimens vary between 0.18-0.28 $N \cdot mm^{-1}$ (Tab. 3), with the mean value of 0.24 $N \cdot mm^{-1}$. The obtained cohesive energy values are comparable to values obtained in other studies performed for determination of fracture properties of Norway spruce. Coureau et al. (2013) cite values of 0.25-0.31 $N \cdot mm^{-1}$ depending on the test performed (where the value of 0.25 $N \cdot mm^{-1}$ corresponds to the DCB test), while Ostapska and Malo (2020) give mean value of 0.25 $N \cdot mm^{-1}$ for wedge splitting test. Therefore, the proposed procedure for determining R curves in this paper can be considered to be successful in evaluation of the cohesive energy of spruce.

Tab. 3: The cohesive energy values.

Specimen	**S1**	**S2**	**S3**	**S4**	**S5**	**S6**	**S7**	**S8**	**S9**	**S10**
G_f ($N \cdot mm^{-1}$)	0.275	0.239	0.181	0.248	0.235	0.231	0.20	0.281	0.230	0.278

Crack opening displacement at the initial crack tip was also read from the DIC recorded images. This displacement was determined by choosing two points at the initial crack tip, positioned at the future crack surfaces, and measuring their distance in each step as the crack opens and propagates. This parameter was necessary for further analysis in order to obtain the cohesive law for the specimens. Energy release rate plotted against crack opening displacement at the initial crack tip once it is differentiated gives the cohesive law of tested wood specimens (Gong et al. 2020):

$$\sigma(\delta^*) = \frac{dG(\delta^*)}{d\delta^*} \tag{3}$$

where: σ - stress, δ* - crack opening displacement at the initial crack tip, *G* - energy release rate.

The cohesive law for tested spruce specimens is given in Fig. 10. This was performed for an average value of the obtained results. Maximum value of nominal stress equals 0.9 $N \cdot mm^{-2}$

from the cohesive law curve, corresponding to the value obtained by Oudjene et al. (2016) from DCB tests. Authors of the mentioned paper modelled the progressive cracking of the notch details of spruce timber beams using the CZM option in Abaqus with parameters obtained from the DCB tests.

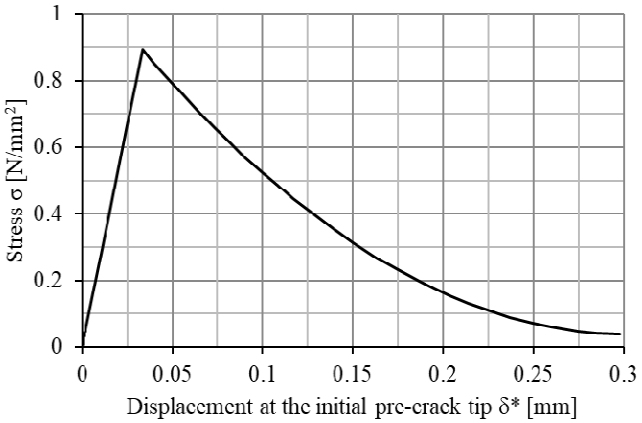

Fig. 10: Cohesive law of tested specimens.

Numerical modelling of end-notched timber beams results

Value of the experimentally obtained cohesive fracture energy and cohesive law was employed for the accurate numerical modelling of damage initiation of end-notched glulam beams. Input data of the damage model in Abaqus are the interface (cohesive) stiffness (K_{nn}, K_{ss}, K_{tt}), the nominal stress values in normal and two shear directions (σ_n, σ_s, σ_t) and the fracture energy (G_f). Nominal stress in normal direction σ_n was taken as maximum value of 0.9 $N \cdot mm^{-2}$ from the cohesive law curve (Fig. 10). Nominal stresses in two shear directions σ_s and σ_t were determined from the experimental tests of wood material properties, values are cited in Tab. 1. The cohesive stiffness value K_{nn} was calculated as the inclination of the linear part of the cohesive law curve given in Fig. 10, determined to be 26.6 $N \cdot mm^{-3}$. In the absence of experimental results, the cohesive stiffness values K_{ss}, K_{tt} were chosen based on parametric analyses conducted with different combinations of cohesive stiffness parameters for the optimal interpretation of the experimental load-displacement curves. The fracture energy was taken as a mean value of DCB test results given below, that is 0.24 $N \cdot mm^{-1}$ (Fig. 9, Tab. 3). The adopted parameters are summarized in Tab. 4.

Tab. 4: Cohesive model parameters

Parameter	**K_{nn} ($N \cdot mm^{-3}$)**	**K_{ss} ($N \cdot mm^{-3}$)**	**K_{tt} ($N \cdot mm^{-3}$)**	**σ_n ($N \cdot mm^{-2}$)**	**σ_s ($N \cdot mm^{-2}$)**	**σ_t ($N \cdot mm^{-2}$)**	**G_f ($N \cdot mm^{-1}$)**
Value	26.6	20.0	20.0	0.9	5.85	5.85	0.24

Mechanical behaviour of tested end-notched beams in terms of load-deflection relationship obtained from the experiments and from the numerical analysis is shown in Fig. 11. Entirely linear elastic behaviour of end-notched beams was recorded. Good agreement between behaviour predicted by the numerical model and experimentally evaluated behaviour for end-notched glulam beams was found. FEM simulated behaviour was also entirely linear elastic, replicating the behaviour of experimentally tested beams.

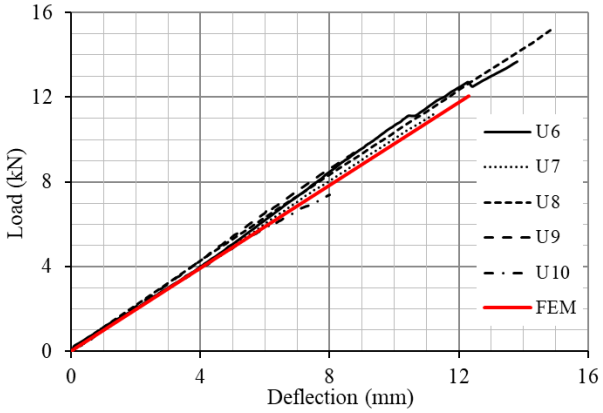

Fig. 11: Experimental and numerical load-deflection curves for end-notched beams.

Experimental and numerical failure modes of the beams are presented in Fig. 12, while the results summary is given in Tab. 5. Experimental results showed that the mechanical properties of tested beams were significantly decreased due notched ends when compared to the expected load-carrying capacity of the beams without notches. The beams failed suddenly and in a brittle manner. In the experimental research, failure was caused by crack opening as a consequence of excessive tensile stress perpendicular to grain, making Mode I clearly dominant fracture mode. When the initial crack opened, its propagation and growth was unstable, leading to a complete separation of the beams in two parts, with generally clear and straight surfaces between two separated parts. FE model showed the same failure type as the tested beams, with dominant Mode I fracture.

Tab. 5: Experimental and numerical results summary.

	Maximum load F_{max} (kN)	**Mid-span deflection w (mm)**	**Bending stiffness EI (x 10^8 kN·mm^2)**
Experimental	12.8 (25.2%*)	11.5 (26.6%*)	9.19 (5.8%*)
Numerical	12.1	12.3	8.93
Difference (%)	5.4	6.5	2.8

*Coefficient of variation.

The difference between the results of maximum load obtained from theoretical model and the experiment is 5.4%. The numerical value of maximum load was determined 12.1 kN in comparison to the experimental value of 12.8 kN. The numerical model estimated the mid-span deflection at maximum load to be 12.3 mm, while the experimental value was 11.5 mm. The difference in the mid-span deflection at maximum load was 6.5%, showing good agreement of the results. The differences can be explained by high coefficient of variation in the experimental results due to natural diverse behaviour of wood as a material. The difference in bending stiffness of the beams between the experimentally and numerically obtained values, 9.19 kN·mm^2 x 10^8 and 8.93 kN·mm^2 x 10^8 respectively, is only 2.8%.

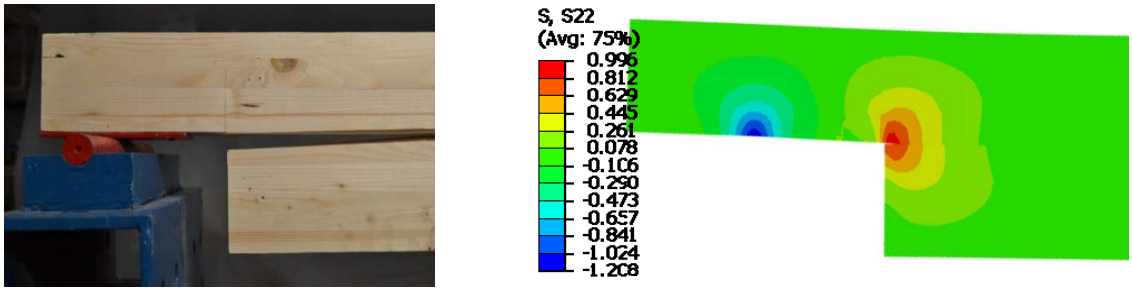

a) *b)*

Fig. 12: Experimental and numerical failure modes of end-notched beams: a) Experimental (at maximum load), b) FEM (σ_{nn} – tensile stress perpendicular to the grain at maximum load).

CONCLUSIONS

There are no standardized procedures to determine wood cohesive law essential for numerical modelling of different structural problems. An efficient test and analysis procedure to obtain the Mode I timber fracture (crack opening) properties based on the DCB tests is proposed in this paper. Based on the obtained results the cohesive energy G_f corresponding to the plateau value of the R curve was determined to be 0.24 $N \cdot mm^{-1}$ for specimens made of European spruce. Furthermore, R curves were analysed in order to obtain cohesive law necessary for numerical modelling of Mode I fracture behaviour of structural beam component made of timber. The proposed method has been proven to be successful in determination of Mode I fracture properties of wood.

Cohesive law was implemented in the numerical analysis of large-scale end-notched glulam beams which were previously tested in four-point bending configuration. The numerical modelling, as well as the experimental research, can help in better understanding of crack initiation and crack growth phenomenon in end-notched timber beams. Comprehending the Mode I fracture in timber allows to determine the expected behaviour of end-notched timber beams in terms of load-carrying capacity, ductility and damage tolerance. Good agreement was found between the proposed numerical solution and experimental results. The presented models can be used for further parametric analyses, which would include varying the loading configuration, geometry and material properties.

ACKNOWLEDGMENT

This research was supported by the Science Fund of the Republic of Serbia, Serbian Science and Diaspora Collaboration Program: Knowledge Exchange Vouchers: Hybrid structures and connection of timber and FRP. The authors express gratitude to personnel of Stevin 2 Laboratory at TU Delft that helped in performing DCB tests with DIC.

REFERENCES

1. Bodig, J., Jayne, B.A., 1982: Mechanics of wood and wood composites. New York: Van Nostrand Reinhold, 736 pp.
2. Coureau, J.L., Morel, S., Dourado, N., 2013: Cohesive zone model and quasibrittle failure of wood: A new light on the adapted specimen geometries for fracture tests. Engineering Fracture Mechanics 109: 328-340.
3. de Moura, M.F.S.F., Morais, J.J.L., Dourado, N., 2008: A new data reduction scheme for mode I wood fracture characterization using the double cantilever beam test Engineering Fracture Mechanics 75(13): 3852-3865.
4. de Moura, M.F.S.F., Dourado, N., 2018: Mode I fracture characterization of wood using the TDCB test. Theoretical and Applied Fracture Mechanics 94: 40-45.
5. Dourado, N., De Moura, M.F.S.F., Morel, S., Morais J., 2015: Wood fracture characterization under mode I loading using the three-point-bending test. Experimental investigation of *Picea abies* L. International Journal of Fracture 194: 1–9.
6. Dubois, F., Méité, M., Pop, O., Absi, J., 2012: Characterization of timber fracture using the Digital Image Correlation technique and Finite Element Method. Engineering Fracture Mechanics 96: 107-121.
7. EN 338, 2009: Structural timber. Strength classes.
8. EN 384, 2010: Structural timber. Determination of characteristic values of mechanical properties and density.
9. EN 408:2010+a1, 2012: Timber structures. Structural timber and glued laminated timber. Determination of some physical and mechanical properties.
10. Gong, Y., Hou, Y., Zhao, L., Li, W., Zhang, J., Hu, N., 2020: A modified mode I cohesive zone model for the delamination growth in DCB laminates with the effect of fiber bridging. International Journal of Mechanical Sciences 176: 105514.
11. ISO 13061-2, 2014: Physical and mechanical properties of wood - Test methods for small clear wood specimens - Part 2: Determination of density for physical and mechanical tests. International Organization for Standardization, Geneva, Switzerland.
12. Jamaaoui, A., Pop, O., Dubois, F., Costa, G., 2017: Wedge splitting test on douglas genotypes using an integrated mixed-mode approach. Theoretical and Applied Fracture Mechanics 91: 44–51.
13. Jockwer, R., 2014: Structural behaviour of glued laminated timber beams with unreinforced and reinforced notches. PhD Thesis. ETH, Zurich, Switzerland, 165 pp.
14. Morel, S., Dourado, N., Valentin, G., Morais, J., 2005: Wood: a quasibrittle material R-curve behavior and peak load evaluation. International Journal of Fracture 131: 385-400.
15. Nairn, J.A., Matsumoto, N., 2009: Fracture modeling of crack propagation in wood and wood composites including crack tip processes and fiber bridging mechanics. In: Proceedings of the 12th international conference on fracture. Pp 3411–3418, Red Hook, NY, USA: Curran Associates, Inc. Ottawa, Canada.
16. Nakao, T., Susanti, C.M.E., Yoshihara, H., 2012: Examination of the failure behavior of wood with a short crack in the radial–longitudinal system by single-edge-notched bending test. Journal of Wood Science 58: 453-458.

17. Ostapska, K., Malo, K.A., 2020: Wedge splitting test of wood for fracture parameters estimation of Norway Spruce. Engineering Fracture Mechanics 232: 107024.
18. Ostapska, K., Malo, K.A., 2021: Crack path tracking using DIC and XFEM modelling of mixed-mode fracture in wood, Theoretical and Applied Fracture Mechanics 112: 102896.
19. Oudjene, M., Tran, V., Meghlat, E., Ait-Aider, H., 2016: Numerical models for self-tapping screws as reinforcement of timber structures and joints. In: Proceedings of 14th World Conference on Timber Engineering 2016. TU Verlag Wien. Vienna, Austria. Pp. 2680-2687.
20. Todorović, M., Glišović, I., Stevanović, B. 2019: Experimental investigation of cracked end-notched glulam beams repaired with GFRP bars. Wood Research 64(6): 1077-1086.
21. Todorović, M., Glišović, I., Stevanović, B., 2022: Experimental investigation of end-notched glulam beams reinforced with GFRP bars. European Journal of Wood and Wood Products 80: 1071-1085.
22. Vasic, S., Smith, I., 2002: Bridging crack model for fracture of spruce. Engineering Fracture Mechanics 69(6): 745-760.
23. Wilson, E., Mohammadi, M.S., Nairn, J. A., 2013: Crack propagation fracture toughness of several wood species. Advances in Civil Engineering Materials 2(1): 316–327.
24. Yoshihara, H., Kawamura, T., 2006: Mode I fracture toughness estimation of wood by DCB test. Composites Part A: Applied Science and Manufacturing 37(11): 2105-2113.
25. Zhao, Y., Li, Z., Xu, B., 2017: Mixed-mode (I/II) interlaminar fracture of glued-laminated timber. Materials & Design 131: 210-218.

MARIJA TODOROVIĆ*, NAĐA SIMOVIĆ, IVAN GLIŠOVIĆ
UNIVERSITY OF BELGRADE
FACULTY OF CIVIL ENGINEERING
DEPARTMENT OF MATERIALS AND STRUCTURES
BULEVAR KRALJA ALEKSANDRA 73, BELGRADE
SERBIA
*Corresponding author: todorovicm@grf.bg.ac.rs

MATHIEU KOETSIER, MARKO PAVLOVIĆ
DELFT UNIVERSITY OF TECHNOLOGY
CIVIL ENGINEERING AND GEOSCIENCES
STEVINWEG 1, 2628 CN DELFT
THE NETHERLANDS